Aerosol Radiative Forcing and Forcing Efficiency in the UVB for Regions Affected by Saharan and Asian Mineral Dust

O. E. GARCÍA, A. M. DÍAZ, F. J. EXPÓSITO, AND J. P. DÍAZ

Grupo de Observación de la Tierra y la Atmósfera, University of La Laguna, La Laguna, Spain

A. REDONDAS

Centro de Investigación Atmosférico de Izaña, Spanish State Meteorological Agency, Izaña, Spain

T. SASAKI

Ozone Layer Monitoring Office, Japan Meteorological Agency, Tokyo, Japan

(Manuscript received 18 April 2008, in final form 25 August 2008)

ABSTRACT

The influence of mineral dust on ultraviolet energy transfer is studied for two different mineralogical origins. The aerosol radiative forcing ΔF and the forcing efficiency at the surface ΔF^{eff} in the range 290–325 nm were estimated in ground-based stations affected by the Saharan and Asian deserts during the dusty seasons. UVB solar measurements were taken from the World Ozone and Ultraviolet Data Center (WOUDC) for four Asian stations (2000–04) and from the Santa Cruz Observatory, Canary Islands (2002–03), under Gobi and Sahara Desert influences, respectively. The Moderate Resolution Imaging Spectroradiometer (MODIS) aerosol optical depth at 550 nm was used to characterize the aerosol load τ, whereas the aerosol index provided by the Total Ozone Mapping Spectrometer (TOMS) sensor was employed to identify the mineral dust events. The ΔF is strongly affected by the aerosol load, the values found being comparable in both regions during the dusty seasons. Under those conditions, ΔF values as large as -1.29 ± 0.53 W m^{-2} ($\tau_{550} = 0.48 \pm 0.24$) and -1.43 ± 0.38 W m^{-2} ($\tau_{550} = 0.54 \pm 0.26$) were reached under Saharan and Asian dust conditions, respectively. Nevertheless, significant differences have been observed in the aerosol radiative forcing per unit of aerosol optical depth in the slant path, τ_S. The maximum ΔF^{eff} values associated with dust influences were -1.55 ± 0.20 W m^{-2} τ_{S550}^{-1} for the Saharan region and -0.95 ± 0.11 W m^{-2} τ_{S550}^{-1} in the Asian area. These results may be used as a benchmark database for establishing aerosol corrections in UV satellite products or in global climate model estimations.

1. Introduction

The importance of the harmful effects of solar ultraviolet radiation (UV) has warranted a significant effort to understand all aspects of the UV radiative transfer in the atmosphere. One of the aspects to be improved is the knowledge of the role played by the atmospheric aerosols, and special attention must be paid to absorbing aerosols such as particles from biomass burning and desert dust. In this context, mineral dust is the major contributor to natural aerosol load on a global scale (Satheesh and Moorthy 2005) and plays a crucial role in radiative processes in the earth–atmosphere system. One of the most important effects is its direct action on the radiative budget, which has been estimated from -0.56 to $+0.1$ W m^{-2} on a global scale (Alley et al. 2007). Recent studies suggest that the local effect can be far stronger, as much as tens or hundreds of W m^{-2} (Alley et al. 2007), principally in those regions where this is the dominant aerosol component.

Nevertheless, the influence of UV still shows considerable uncertainties, which can become potential error sources, especially in UV measurements from satellite products or in global climate models. For instance, under cloud-free conditions the accuracy of satellite UV estimations is limited mainly by the knowledge of highly variable aerosol properties (Krotkov et al. 1998; WMO

Corresponding author address: Omaira E. García, Grupo de Observación de la Tierra y la Atmósfera, University of La Laguna, 38207 La Laguna, Spain.
E-mail: ogarcia@ull.es

DOI: 10.1175/2008JAS2816.1

2003). In particular, the effect of aerosols on UV satellite products (e.g., total ozone content or UV maps) over large areas is greater where the largest dust concentrations are found, such as Saharan plumes (Herman et al. 2001; Torres and Bhartia 1999).

The physical and optical properties of the atmospheric aerosols directly depend on the source regions and on the modifications that occur during the transport history. In the case of mineral dust, the two main source areas are the Saharan–Sahel and Asian deserts (the Taklimakan and Gobi Deserts), which show different mineralogical characteristics (Sokolik and Toon 1999; Arimoto et al. 2006; Shen et al. 2006) and hence different radiative traces. In particular, Sokolik and Toon (1999) found that aerosol optical properties are very sensitive to the individual minerals and their mixtures in dust composition, even modifying the net effect (i.e., the sign) of mineral dust radiative forcing. Thus, the present study examines the impact of the natural mineral dust on the UV energy transfer by analyzing the influence of the source region.

2. Instrumentation and database

To characterize the aerosol load, remote sensing techniques are one of the most useful tools covering the spatial and temporal distribution of these atmospheric constituents. To this end, the daily aerosol optical depth τ, averaged over ocean and land, at 550 nm provided by the Moderate Resolution Imaging Spectroradiometer (MODIS) sensor on board *Terra* has been used in the current study. The MODIS data corresponds to level-2 aerosol products MOD04_L2. This magnitude has been widely validated both in dusty and nondusty regimes (Remer et al. 2005 and references therein), showing an uncertainty range of $\Delta\tau = \pm 0.03 \pm 0.05\tau$ over ocean and $\Delta\tau = \pm 0.05 \pm 0.15\tau$ over land. Figure 1 depicts an example of the MODIS τ during mineral dust events over the study areas (the locations of the ground-based stations are also shown). To complete the aerosol characterization and identify the mineral dust events, we have also considered the daily aerosol index (AI) measurements provided by the Total Ozone Mapping Spectrometer (TOMS) sensor on board the *Earth Probe* satellite. Positive values of this parameter indicate the presence of UV-absorbing aerosols (Torres et al. 1998), which in the studied region consist mainly of mineral dust. Thus, these scenarios are identified with AI values higher than 1 (overpass, version 8; http://toms.gsfc.nasa.gov).

With regard to the solar database, the spectral global UVB irradiance was measured by Brewer instruments (MKII and MKIII) at the World Ozone and Ultraviolet Data Center (WOUDC) stations from 2000 to 2004 and integrated in the range of 290–325 nm. The ultraviolet data follow specific calibration procedures (http://www.kousou-jma.go.jp/), with an unexpected uncertainty less than $\pm 3\%$. For the Saharan location, the spectral irradiance, also in the range of 290–325 nm, was measured during 2002 and 2003 by a Bentham DM 150 spectroradiometer belonging to the University of La Laguna and installed at the facilities of the Centro de Investigación Atmosférico de Izaña (Spanish State Meteorological Agency; http://www.aemet.es). Quality control and quality assurance have been tested by comparing this instrument with, among others, the UV European standard [the Quality Assurance of Solar Ultraviolet Spectral Irradiance Measurements (QASUME)], showing differences of less than 5% (Díaz et al. 2008, manuscript submitted to *Geophys. Res. Lett.*).

The spatial and temporal collocation between ground-based solar data and remote sensing measurements (τ-MODIS and AI–TOMS) was made taking into account the criterion outlined by Remer et al. (2005). This approach establishes a MODIS average in a box of 50×50 km^2 ($\sim \pm 0.25°$) centered in each station, and the ground-based measurement (UVB radiative forcing data) is averaged within ± 1 h of satellite overpass, which is located around the daily local noon. This ensures that the analysis is limited to solar zenith angles (SZAs) less than 60°, thus avoiding measurement errors of the UV spectroradiometers at large SZAs (cosine effect). The same methodology was employed with the AI measurements. To avoid UV enhanced by the presence of snow, the winter months have been avoided and only the months from March to November have been used in this work. The cloud-free conditions were determined from the fit to a Gaussian function of the integrated global irradiance along the whole day (García et al. 2006). Only days with a correlation coefficient higher than 0.98 were selected. Overcast days might pass this filter, but these uniform cloud conditions are ruled out because the solar database was matched with MODIS aerosol optical depth, retrieved only under cloudless sky situations (Remer et al. 2005).

3. Site descriptions

To compare the influence on UV of the two main mineral sources of desert dust, several stations affected by the transport of Asian and Saharan dust plumes were selected: four Asian locations—Kagoshima (KAG), Sapporo (SAP), Tateno (TAT), and Naha (NAH), all in Japan—all of which belong to the WOUDC network (http://www.woudc.org), and Santa Cruz de Tenerife station (SCO), located in the Canary Islands and managed by the Centro de Investigación Atmosférico de

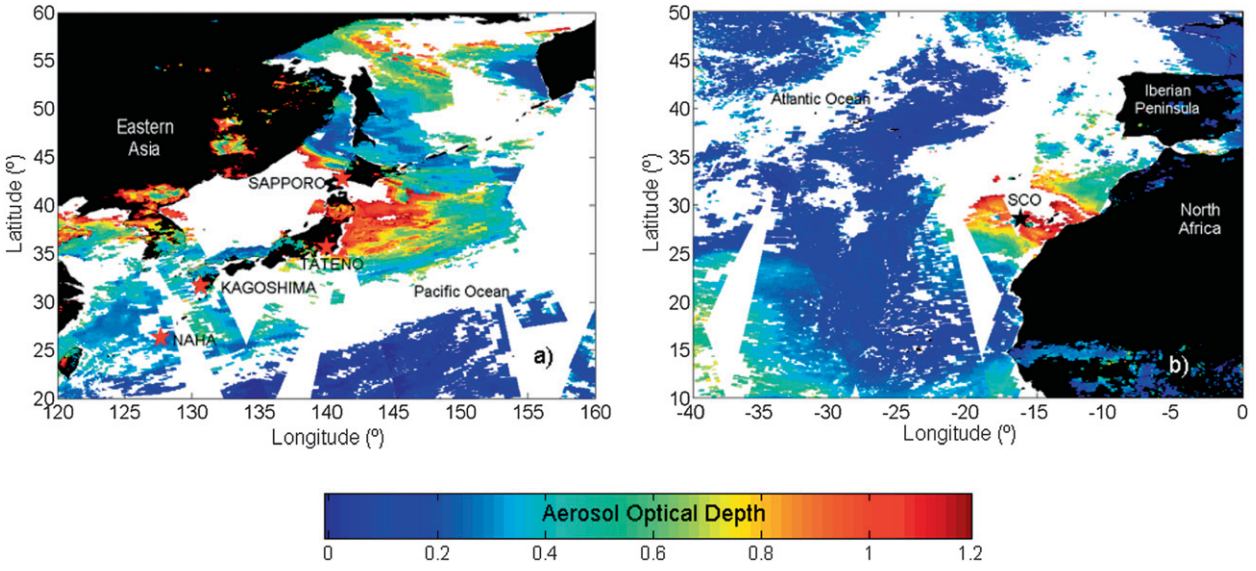

FIG. 1. MODIS aerosol optical depth at 550 nm during mineral dust events at (a) 10 May 2003 for Asian locations and (b) 5 Oct 2002 for Santa Cruz de Tenerife station (SCO). The location of the ground-based stations is also shown.

Izaña. The description of these stations is shown in Table 1, where information about the main aerosol influences is also given. The dust transport over the selected stations has a strong seasonal behavior, showing a different pattern across the Atlantic and the Pacific Oceans depending on the season. The main period for dust presence in the Asian region is during the spring (Sun et al. 2001; Kim et al. 2004; Chu et al. 2005), whereas in the northeast subtropical Atlantic region the dust presence is stronger in the winter and summer seasons, although dust events are observed all year (García et al. 2009, and references therein). Unlike Saharan dust outbreaks affecting the Canaries that are dominated by fresh dust particles, Asian dust plumes are often mixed with urban/industrial pollutants and biomass burning aerosols (Conant et al. 2003; Chu et al. 2005; Arimoto et al. 2006).

The monthly mean of the MODIS aerosol optical depth at 550 nm by station is shown in Fig. 2. Notice that the available datasets for each site, listed in Table 1, result from the temporal collocation between the satellite overpass and the solar database, excluding the winter months. As was noted previously, an elevated aerosol load is clearly seen in the springtime for Japanese stations, where from April to June the largest monthly averages are found. Thus, the annual maximum τ_{550} is reached in April for Naha and Sapporo (0.48 ± 0.24 and 0.53 ± 0.26, respectively), whereas for Kagoshima and Tateno mean values as large as 0.43 ± 0.23 and 0.59 ± 0.30, respectively, are obtained in June. Additionally, in this season the highest variation of τ_{550} values (see the standard deviation of the mean value) is found, to which Asian dust outbreaks contribute significantly. In fact, in this season the annual maximum frequency of occurrences with AI > 1 has been observed, which ranges from 40% in Naha up to 47% in Tateno.

Except for Naha, the summer period shows the second largest values; the lowest seasonal means occur during the autumn. Yamazaki et al. (1999) found that the seasonal difference in the amount of Asian dust particles between northern and central-southern Japan is due to the effects of the summer monsoon. Naha is the most southern of the Asian stations, located in a maritime environment in tropical Southeast Asia, and it is strongly affected by the cleaning atmospheric processes associated with the wet Asian monsoon. Thus, the lowest annual values are reached during the summer season: 0.16 ± 0.10 in August. From Japanese stations, Naha is the only location affected frequently by biomass burning as result of agricultural clearing in northwestern China (Chu et al. 2005). Hence, aerosol mixtures of biomass burning and, to a lesser degree, desert dust are expected in this station during springtime.

Regarding the SCO station, the largest monthly average τ_{550} values are observed in the summer season with a maximum of 0.37 ± 0.25 in July, which corresponds to one of the annual peaks of Sahara desert activity. In this month 71% of the cases with AI > 1 are assembled, which represents 48% of the all registered cases during this season. In addition, significant τ_{550} values were found in October, 0.26 ± 0.23. As mentioned before, the Canary Islands region also is strongly affected by mineral dust events in the winter season,

TABLE 1. Description of the stations in terms of location (latitude, longitude, and altitude) and aerosol influences. Here N is the total number of available data for each site during the common period MODIS/TOMS-UV data, which have verified the temporal constriction (±1 h) between solar measurements and satellite overpass (MODIS and TOMS). The winter months, from December to February, have been excluded.

Station	Country	Latitude (°)	Longitude (°)	Altitude (m)	Aerosol influence(s)	Period	N
Sapporo (SAP)	Japan	43.05	141.33	19	Asian dust pollution	2000–04	304
Tateno (TAT)	Japan	36.05	140.13	31		2000–04	416
Kagoshima (KAG)	Japan	31.63	130.60	283		2000–04	362
Naha (NAH)	Japan	26.20	127.67	29	Primarily maritime pollution and biomass burning Asian dust	2000–04	192
Santa Cruz de Tenerife (SCO)	Spain	28.47	−16.25	52	Maritime Saharan–Sahel dust	2002–03	146

although in the present study there are not enough available data that show this transport. Note that, on average, the aerosol load levels found at SCO are smaller than those observed at the Japanese stations because of the high pollution background in the Asian locations. In contrast, SCO mainly has a significant contribution of natural particles, Saharan dust, and maritime aerosols (García et al. 2009; Díaz et al. 2008, manuscript submitted to *Geophys. Res. Lett.*).

4. UVB aerosol radiative forcing and forcing efficiency

Aerosol radiative forcing ΔF is defined as the difference between the global solar irradiance with and without aerosols present:

$$\Delta F = F_{\text{aer}} - F, \tag{1}$$

where F_{aer} and F are the solar fluxes at the surface, integrated between 290 and 325 nm, with and without aerosols respectively. This sign criterion implies that negative (positive) values of ΔF are associated with an aerosol cooling (warming) effect. The solar fluxes with aerosols are measured as described before, whereas the aerosol-free irradiance is computed with the UVSPEC transfer model (Kylling et al. 1995), following the methodology described by García et al. (2006). The main concern in the simulation of the UVB radiation levels is to consider the total ozone content accurately. Thus, to minimize to uncertainty resulting from this fact, we have used the daily ozone content retrieved by Brewer spectroradiometers. For the Asian stations, the ozone

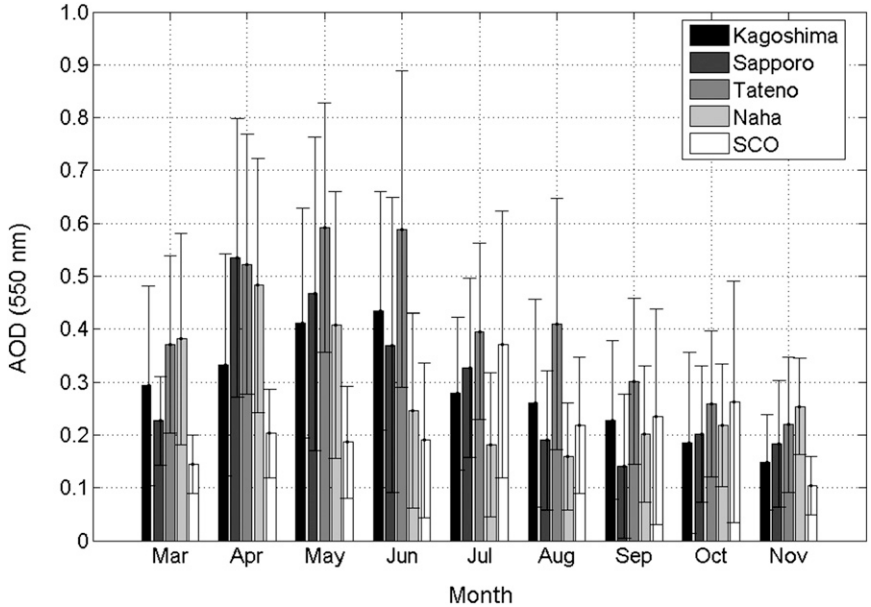

FIG. 2. Monthly mean of the MODIS aerosol optical depth at 550 nm for the studied period of 2000–04 for the Asian stations and 2002–03 for SCO.

content was provided by WOUDC, whereas for SCO the values were obtained from the Brewer spectroradiometer managed by the Centro de Investigación Atmosférico de Izaña (Redondas 2007). The gaps of both databases were covered with the ozone TOMS overpass over each ground-based station (http://toms.gsfc.nasa.gov/ozone/). Finally, the standard vertical profile, taken from Anderson et al. (1987), was scaled to match the measured ozone in a column.

Mayer et al. (1997) found that, for UVSPEC simulations, the expected uncertainties on solar fluxes without aerosols are lower than 10% in the UVB spectral range. Together with experimental uncertainties, lower than 5%, we could assume errors lower than 15% for the aerosol radiative forcing values.

As can be observed in Fig. 3, the aerosol radiative forcing follows the behavior observed in the monthly evolution of the aerosol optical depth (Fig. 2): the annual maximum ΔF values are associated with maximum aerosol load. To identify mineral dust events in both regions and compare the UVB radiative effect, only those episodes with AI > 1 have been selected. In these conditions, the number of data decrease up to 36% for SCO and between 12% and 21% for the Asian stations (12% KAG, 15% NAH, 16% TAT, and 21% SAP) compared to the total data shown in Table 1.

For the Asian stations, the highest annual ΔF values are reached during the spring and at the beginning of summer season because of the increase in aerosol levels associated with mineral dust presence. In Sapporo, the northern station, a mean ΔF of -1.19 ± 0.44 W m^{-2} ($\tau_{550} = 0.60 \pm 0.34$, the seasonal average of aerosol optical depth) was observed during the dusty season, although similar ΔF values were found in summer, up to -1.13 ± 0.41 W m^{-2} ($\tau_{550} = 0.45 \pm 0.29$), when mixture processes between local pollution and occasional Siberian forest fires could be responsible for this enhancement (Aoki and Fujiyoshi 2003).

Tateno and Kagoshima are located in the main dust transport routes (Sun et al. 2001), where the mineral dust is directly transported from the Gobi desert. For Kagoshima the springtime shows the most significant ΔF values, -1.43 ± 0.38 W m^{-2} ($\tau_{550} = 0.54 \pm 0.26$), whereas values up to -1.19 ± 0.34 W m^{-2} ($\tau_{550} = 0.62 \pm 0.26$) were obtained during this season in Tateno. Nevertheless, for Tateno the annual maximum was reached in summer, when the secondary peak in the aerosol load occurs, as in Sapporo. This station is located in the proximity of the metropolitan area of Tokyo; therefore, local phenomena and pollution transports are the most likely aerosol source in these months, together with sporadic dust events.

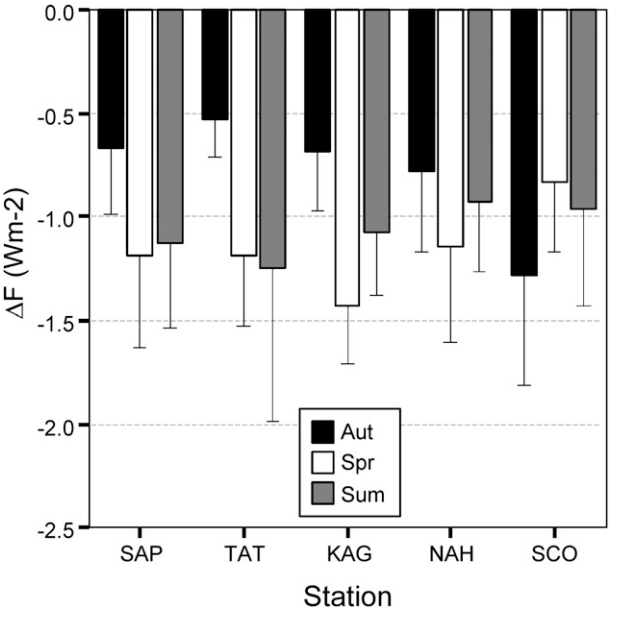

FIG. 3. Seasonal mean of the aerosol radiative forcing ΔF (W m^{-2}) for the studied period, considering only those episodes with AI > 1. The error assigned to each mean value is the standard deviation.

Special attention must be paid to Naha station, where the highest ΔF values found during the spring season could be associated to the possible mix of mineral dust and other aerosols such as urban/industrial or biomass burning aerosols. Note that this last aerosol is also UV absorbing, showing AI > 1, and thus is indiscernible from mineral dust, considering only AI and τ information.

Regarding SCO, seasonal ΔF values as large as -0.96 ± 0.46 and -1.29 ± 0.53 W m^{-2} were reached in summer and autumn respectively, when a high aerosol load due to mineral dust was observed: 0.30 ± 0.23 and 0.48 ± 0.24. Notice that the ΔF values in both the Asian and Atlantic regions are comparable, with the aerosol load being slightly smaller in SCO location.

The aerosol radiative forcing is strongly affected by the aerosol load, among other factors; hence, the analysis of aerosol radiative forcing efficiency ΔF^{eff} becomes a very useful tool. This magnitude allows us to evaluate the direct radiative effect of each type of aerosol, characterized by a size distribution and chemical composition, because the influence of the aerosol load is ruled out. The magnitude is defined as the rate at which the atmosphere is forced, $\Delta(\Delta F)$, per unit of aerosol optical depth $\Delta\tau$ at 550 nm:

$$\Delta F^{\text{eff}} = \Delta(\Delta F)/\Delta\tau_{550}. \quad (2)$$

This magnitude, under cloudless and snow-free conditions at the surface, was calculated through the slope

method (Jayaraman et al. 1998; Bush and Valero 2003) by seasons, using a least squares linear fit. To this aim, the instantaneous aerosol optical depth was divided by the cosine of solar zenith angle, giving the aerosol optical depth in slant τ_s, to account for the effect of the optical path (García et al. 2006). As for the ΔF analysis, only days with AI > 1 have been considered. Figure 4 shows two examples of the slope method for stations affected by Asian and Saharan dust, respectively: Tateno and SCO. The errors in the ΔF are propagated to the ΔF^{eff}, and as can be observed in Table 2 where the ΔF^{eff} values during the dusty seasons are listed, the uncertainties range between 11% and 25% except for SCO in autumn, where an error of ~50% was found.

Although ΔF^{eff} is defined for an aerosol optical depth at 550 nm, sensitivity tests show differences less than 15% in the radiative forcing estimations from ΔF^{eff} evaluated with τ_s at 550 and 320 nm during dusty seasons in both regions. The ΔF^{eff} at 320 nm was estimated from the MODIS aerosol product over land (with aerosol optical depth of 470, 550, and 660 nm), assuming an Ångström power law for the τ spectral dependence. Therefore, we have kept the traditional definition to be consistent with the literature and facilitate future comparisons.

Except at Naha, the seasonal ΔF^{eff} values obtained during the mineral dust seasons are larger at SCO than at the Japanese stations, demonstrating a higher Saharan dust attenuation capability in the UVB spectral region per unit of aerosol optical depth. Thus, values as large as -1.55 ± 0.20 and -1.13 ± 0.58 W m^{-2} τ_{S550}^{-1} were reached in summer and autumn respectively, when the maximum aerosol load observed was due to mineral dust; whereas in Japanese stations, ΔF^{eff} values up to -0.95 ± 0.11 W m^{-2} τ_{S550}^{-1}, obtained at Tateno, were associated with dust influences. For Naha, the ΔF^{eff} reached -1.38 ± 0.36 W m^{-2} τ_{S550}^{-1} in spring, but as noted previously this value could be associated with the combined effect of mineral dust and biomass burning.

The seasonal differences observed at SCO can be associated with the dust vertical distribution (Díaz et al. 2000), which is strongly linked to the synoptic meteorological pattern in this subtropical Atlantic region. Thus, the dust transport in cold season occurs mainly at low altitudes, within the marine boundary layer where SCO is located, whereas in summer the dust is transported above 2 km MSL (Díaz et al. 2000; García et al. 2009).

A key feature explaining the different values found at SCO and the Asian stations is the possible moderation of ΔF^{eff} values due to different mineralogical composition, especially the amount of iron oxides (hematite, goethite, etc.) present in the aeolian dust. These minerals, especially hematite, are strongly absorbent of UV and visible wavelengths; further, they enhance the absorption of other dust components, such as clay minerals and quartz, forming aggregates and strongly modifying the dust optical properties (Sokolik and Toon 1999; Kalashnikova and Sokolik 2002). Recent studies show that Asian dust mixtures contain relatively lower concentrations of iron oxides in the form of hematite than Saharan dust, so the effective absorption of the Asian dust is expected to be lower per unit mass (Kalashnikova and Sokolik 2002; Shen et al. 2006; Arimoto et al. 2006). For instance, an imaginary refractive index of -9×10^{-3} was retrieved for Saharan dust from mineralogical data, whereas values near -3×10^{-4}, or even lower, were recorded for Asian mineral dust at the midvisible solar spectrum (Arimoto et al. 2006; Kandler et al. 2007).

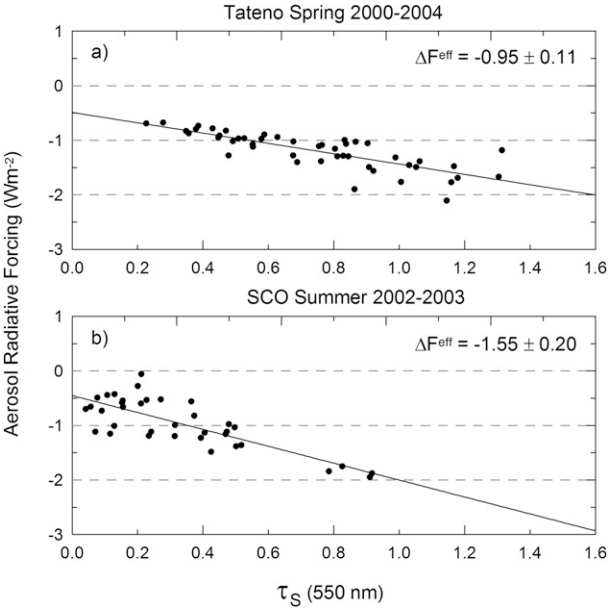

FIG. 4. Aerosol radiative forcing ΔF (W m^{-2}) vs aerosol optical depth in slant path τ_S at 550 nm for (a) Tateno and (b) SCO during dusty seasons, considering only those episodes with AI $>$ 1. The correlation coefficient of the linear fit is 80% in both cases.

In addition, the mixing state of the mineral dust in each region must be taken into account. As noted previously, Asian dust plumes are often mixed with urban/industrial pollutants and biomass burning aerosols. As a result, the internal mixing of fine aerosols, principally black carbon, with dust particles significantly enhances the absorption properties during Asian dust events, especially in the submicrometer range. Arimoto et al. (2006) also found an imaginary refractive index of -6×10^{-4} for polluted dust. Aerosol radiative properties, such as single scattering albedo ω, also show the modification of the dust properties during dust transport over urban/industrial areas. After interacting with pollution, dust can reach small values of ω (e.g., $\omega < 0.90$ or even

TABLE 2. Aerosol radiative forcing efficiency, ΔF^{eff} (W m^{-2} τ_{S550}^{-1}) during the dusty seasons for each region: spring for the Asian stations and summer and autumn for SCO. The range of aerosol optical depth in the slant path used to evaluate the ΔF^{eff}, $\Delta\tau_{S550}$, is also given. The error assigned to ΔF^{eff} is the standard deviation of the slope of linear fit.

Station	ΔF^{eff}	$\Delta\tau_{S\ 550}$	Season
Sapporo	-0.88 ± 0.10	0.2–1.8	Spring
Naha	-1.38 ± 0.36	0.2–0.9	
Kagoshima	-0.69 ± 0.17	0.2–1.4	
Tateno	-0.95 ± 0.11	0.2–1.3	
SCO	-1.55 ± 0.20	0.0–1.0	Summer
	-1.13 ± 0.58	0.2–1.0	Autumn

as low as 0.81), which contrasts strongly with ω values of fresh dust particles over the East Asia continent: ~0.90, or up to 0.95 to 0.98 at 500 nm observed in the Sea of Japan (Conant et al. 2003; Kim et al. 2004). Therefore, an increment in the radiative differences between regions could be expected for stations closer to the mineral dust sources, where the mixture processes are lower.

Most radiative studies are carried out considering the aerosol radiative effects on the whole solar spectrum; hence, their results are not comparable to individual spectral ranges and specifically to UV wavelengths. Nevertheless, similar results were found by García et al. (2006), for example, when the UVB effects of background and urban/industrial aerosols were analyzed. In that study, the ΔF^{eff} values for the background stations range from -0.24 ± 0.17 to -2.07 ± 0.62 W m^{-2} τ_{S550}^{-1}, which are comparable to ones found under mineral dust conditions in the present work, whereas the aerosol load is significantly smaller. This behavior results, on the one hand, from the different aerosol radiative characteristics, and on the other hand it could be attributed to the effect described by Conant et al. (2003). This latter work shows that the aerosol forcing efficiency is modulated by the aerosol load; that is, ΔF^{eff} values are higher when $\tau \ll 1$ because of the increase of multiple scattering effects and attenuation of the transmitted radiation for large τ. In urban/industrial environments, ΔF^{eff} results were found to be similar to the nondusty season, when the UVB attenuation by atmospheric aerosols is smaller (García et al. 2006).

5. Summary and conclusions

The direct radiative effect of desert dust on UVB irradiance levels was evaluated by means of the aerosol radiative forcing ΔF and forcing efficiency ΔF^{eff}, combining surface solar measurements and remote sensing information (aerosol optical depth from MODIS and aerosol index from TOMS). The influence of source region was analyzed, selecting measurement stations affected by mineral dust transports from the strongest desert dust area, the Sahara–Sahel and Gobi deserts. Here, ΔF estimations show that both regions have comparable net effect on UVB spectral range, although Saharan dust has the highest attenuation capability in the UVB per unit of aerosol optical depth. These different radiative traces could be associated with the different physical and chemical properties in their origins. Nevertheless, special attention must be paid to the mixture processes in Asian dust transport because the mixing with local pollution and biomass burning significantly enhances the Asian dust absorption efficiency. This is very critical in the estimations of UV trends. Eastern Asia emits large amounts of urban/industrial aerosols, including black carbon, derived from increasing industrial development. Therefore, any changing profile of pollution emissions could have important implications for climate.

In conclusion, the methodology developed combining ground-based and satellite measurements has been shown to be an adequate tool to estimate the radiative transfer of atmospheric aerosols and is suitable to extend the analysis to different aerosol regimes. Nevertheless, further studies are necessary to establish more significant results.

Acknowledgments. We acknowledge the MCYT (Ministry of Science and Technology, Spain) and F.E.D.E.R. foundations (E.U.) for their economic support of projects CGL2004-05984-C07-05, CGL2005-03428-C04-02, CGL2007-66477-C02-02/CLI, CGL2008-04740/CLI and PI042005/033. Also, we acknowledge the data supplied by the MODIS and TOMS teams. The Japanese UV data were obtained from the World Ozone and Ultraviolet Radiation Data Centre (WOUDC) operated by Environment Canada, Toronto, Ontario, Canada under the auspices of the World Meteorological Organization. Finally, the authors wish to express their appreciation to the operators of IZO and WOUDC stations for their help with running the instruments.

REFERENCES

Alley, R. B., and Coauthors, 2007: Summary for policymakers. *Climate Change 2007: The Physical Science Basis,* S. Solomon et al., Eds., Cambridge University Press, 21 pp.

Anderson, G. P., S. A. Clough, F. X. Kneizys, J. H. Chetwynd, and E. P. Shettle, 1987: AFGL atmospheric constituent profiles (0–120 km). AFGL-TR-86-0110 (OPI), Hanscom Air Force Base, 43 pp.

Aoki, K., and Y. Fujiyoshi, 2003: Sky radiometer measurements of aerosol optical properties over Sapporo, Japan. *J. Meteor. Soc. Japan,* **81,** 493–513.

Arimoto, R., and Coauthors, 2006: Characterization of Asian dust during ACE-Asia. *Global Planet. Change,* **52,** 23–56.

Bush, B. C., and F. P. J. Valero, 2003: Surface aerosol radiative forcing at Gosan during the ACE-Asia campaign. *J. Geophys. Res.,* **108,** 8660, doi:10.1029/2002JD003233.

Chu, D. A., and Coauthors, 2005: Evaluation of aerosol properties over ocean from Moderate Resolution Imaging Spectroradiometer (MODIS) during ACE-Asia. *J. Geophys. Res.,* **110,** D07308, doi:10.1029/2004JD005208.

Conant, W. C., and Coauthors, 2003: A model for the radiative forcing during ACE-Asia derived from CIRPAS Twin Otter and R/V *Ronald H. Brown* data and comparison with observations. *J. Geophys. Res.,* **108,** 8661, doi:10.1029/2002JD003260.

Díaz, J. P., F. J. Expósito, C. J. Torres, V. Carreño, and A. Redondas, 2000: Simulation of the mineral dust effects on UV radiation levels. *J. Geophys. Res.,* **105,** 4979–4991.

García, O. E., A. M. Díaz, F. J. Expósito, J. P. Díaz, J. Gröbner, and V. E. Fioletov, 2006: Cloudless aerosol forcing efficiency in the UV region from AERONET and WOUDC databases. *Geophys. Res. Lett.,* **33,** L23803, doi:10.1029/2006GL026794.

——, ——, F. J. Expósito, J. P. Díaz, M. D. Gelado, and C. Guirado, 2009: A methodology to evaluate the aerosol effective radius based on MODIS aerosol products applicable to other satellite platforms. *Int. J. Remote Sens.,* in press.

Herman, J. R., E. Celarier, and D. Larko, 2001: UV 380 nm reflectivity of the Earth's surface, clouds and aerosols. *J. Geophys. Res.,* **106,** 5335–5351.

Jayaraman, A., D. Lubin, S. Ramachandran, V. Ramanathan, E. Woodbridge, W. D. Collins, and K. S. Zalpuri, 1998: Direct observations of aerosol radiative forcing over the tropical Indian Ocean during the January–February 1996 pre-INDOEX cruise. *J. Geophys. Res.,* **103,** 13 827–13 836.

Kalashnikova, O. V., and I. N. Sokolik, 2002: Importance of shapes and compositions of wind-blown dust particles for remote sensing at solar wavelengths. *Geophys. Res. Lett.,* **29,** 1398, doi:10.1029/2002GL014947.

Kandler, K., and Coauthors, 2007: Chemical composition and complex refractive index of Saharan mineral dust at Izaña, Tenerife (Spain) derived by electron microscopy. *Atmos. Environ.,* **41,** 8058–8074.

Kim, D.-H., B.-J. Sohn, T. Nakajima, T. Takamura, T. Takemura, B.-C. Choi, and S.-C. Yoon, 2004: Aerosol optical properties over East Asia determined from ground-based sky radiation measurements. *J. Geophys. Res.,* **109,** D02209, doi:10.1029/2003JD003387.

Krotkov, N. A., P. K. Bhartia, J. R. Herman, V. Fioletov, and J. Kerr, 1998: Satellite estimation of spectral surface UV irradiance in the presence of tropospheric aerosols. 1. Cloud-free case. *J. Geophys. Res.,* **103,** 8779–8793.

Kylling, A., K. Stammes, and S.-C. Tsay, 1995: A reliable and efficient two-stream algorithm for spherical radiative transfer: Documentation of accuracy in realistic layered media. *J. Atmos. Chem.,* **21,** 115–150.

Mayer, B., G. Seckmeyer, and A. Kylling, 1997: Systematic long-term comparison of spectral UV measurements and UVSPEC modelling results. *J. Geophys. Res.,* **102,** 8755–8767.

Redondas, A., 2007: Ozone absolute calibration: Langley regression method. *Proc. World Meteorological Organization Global Atmosphere Watch, 10th Biennial WMO Consultation on Brewer Ozone and UV Spectrophotometer Operation, Calibration and Data Reporting,* Northwich, United Kingdom, WMO, 18–20.

Remer, L. A., and Coauthors, 2005: The MODIS aerosol algorithm, products, and validation. *J. Atmos. Sci.,* **62,** 947–973.

Satheesh, S. K, and K. K. Moorthy, 2005: Radiative effects of natural aerosols: A review. *Atmos. Environ.,* **39,** 2089–2110.

Shen, Z. X., and Coauthors, 2006: Spectroscopic analysis of iron-oxide minerals in aerosol particles from northern China. *Sci. Total Environ.,* **367,** 899–907.

Sokolik, I. N., and O. B. Toon, 1999: Incorporation of mineralogical composition into models of the radiative properties of mineral aerosol from UV to IR wavelengths. *J. Geophys. Res.,* **104,** 9423–9444.

Sun, J., M. Zhang, and T. Liu, 2001: Spatial and temporal characteristics of dust storms in China and its surrounding regions, 1960–1999: Relations to source area and climate. *J. Geophys. Res.,* **106,** 10 325–10 333.

Torres, O., and P. K. Bhartia, 1999: Impact of tropospheric aerosol absorption on ozone retrieval from backscattered ultraviolet measurements. *J. Geophys. Res.,* **104,** 21 569–21 577.

——, ——, J. R. Herman, Z. Ahmad, and J. Gleason, 1998: Derivation of aerosol properties from satellite measurements of backscattered ultraviolet radiation: Theoretical basis. *J. Geophys. Res.,* **103,** 17 099–17 110.

WMO, 2003: Scientific assessment of ozone depletion 2002: Global ozone research and monitoring project. WMO Rep. 47, 498 pp.

Yamazaki, K., H. Yanagihara and K. Aoki, 1999: Simulation of generation and transport of Kosa aerosols. *Special Reports on the Regional Studies of Northeast Eurasia and North Pacific in Hokkaido University,* M. Fukuba, Ed., Hokkaido University, 75–83.